

# Modeling of microstructures in dissimilar copper/stainless steel electron beam welds

I.Tomashchuk\*, P. Sallamand , J.-M. Jouvard.

Institut Carnot de Bourgogne, Université de Bourgogne, 12 rue de la Fonderie 71200 Le Creusot, FRANCE

\* iryna.tomashchuk@u-bourgogne.fr

**Abstract:** This work is dedicated to modeling of element distribution in microstructures of electron beam AISI 316L stainless steel/copper heterogeneous welds. Reproducing real geometry of these microstructures and using data on the properties of Fe/Cu-system, we have created heat transfer/diffusion coupled models to demonstrate development of concentration field of elements during solidification of melted zone. The data on local elemental analysis by SEM-ESD have been used to impose initial conditions and to validate the models.

**Keywords:** electron beam welding, Fe/Cu system, microstructures, undercooling, diffusion.

## 1. Introduction

At the case of electron beam welding of copper with stainless steel two principal case of welding pool morphology are possible <sup>(1)</sup>: 1) droplet-like microstructure: under low acceleration voltage electron beam deviates to the copper side due to thermoelectric effect, so the volume of molten copper is much bigger that steel, and so the brazing of solid steel by the flux of melted copper happens and results on formation of steel drops in copper media; 2) emulsion-like microstructure: under high accelerating voltage, when beam deviation is neglected and the volumes of melted materials are closely equal, the appearance of two non-miscible copper-rich and steel-rich regions resulting on formation of complex structures at the heterogeneous interfaces.

The aim of present modeling is to confirm several hypotheses on the mechanism of formation of these structures, and to compare the dynamics of their development in time during solidification of melted zone. We use the results of SEM-ESD analysis to impose initial conditions of chemical composition and to validate the model by comparing variations on experimental and calculated elemental profiles and diffusion distances.

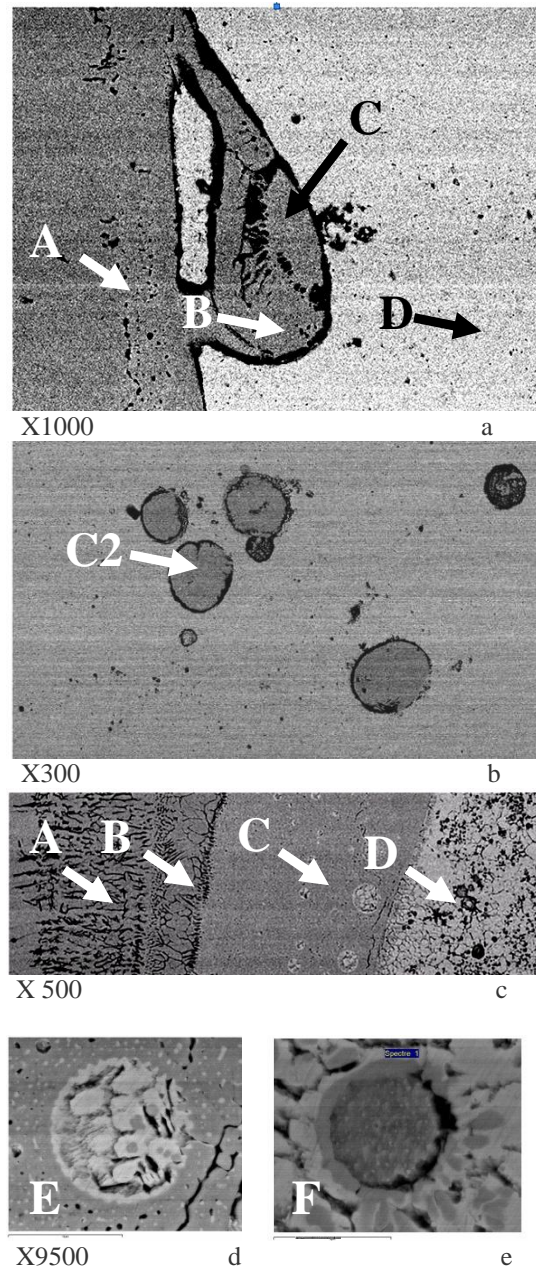


**Figure 1.** The microstructures: droplet (a, b); emulsion-like (c,d,e) joints.

## 2. Experimental data

As an example, two joints with typical microstructure where studied: “droplet”-like joint with  $I = 40$  mA,  $U = 25$  kV,  $P = 1000$  W and “emulsion”-like joint with  $I=30$  mA,  $U = 37,5$  kV,  $P = 1125$  W and 600 mm/min welding speed for both (where  $I$  is beam current,  $U$  is accelerating voltage and  $P=I \cdot U$  is common beam power).

The local elemental SEM-ESD analysis has been carried out to determine composition of present microstructures (Table 1).

To make the hypothesis about phases, which are present in these structures, the solubility of copper in austenitic stainless steel and global solubility of steel in copper have been calculated using additivity rule.  $S_{Cu} = \%Fe \cdot S_{\gamma(max)} + \%Cr \cdot S_{Cr} + \%Ni \cdot S_{Ni} = 18\%$ ;  $S_{steel} = \%Fe \cdot S_{Fe(max)} + \%Cr \cdot S_{Cr(max)} + \%Ni \cdot S_{Ni} = 13\%$ , when the solubility of Fe is only 2,8 at. %. The correspondent phase diagram data has been taken from (2).

The present morphologies (Figure 1) can be divided by: 1) A-structures formed by diffusion of Cu in solid steel, 2) the structures formed by diffusion of Cu in austenitic structure (unsaturated B unmixible with saturated C), 3) little steel-rich structures: C2 (Figure 1,b) with composition equal to C and F (saturated by Cu) (Figure 1,f) containing 15 at. % Cu, 4) little copper-rich structure (Figure 1,e) containing 5,6 at.% Fe (supersaturated).

We suppose that, in the case of droplet-like weld, the steel droplets (Figure 1, a) are tearing away from eroding steel-side by copper-rich flux and form the spheres (about 30  $\mu$ m in diameter).

In the case of emulsion-like weld, we observe several structures formed, as we suppose, due to undercooling phenomena (Figure 1,c-e), which is known for Fe/Cu system (Figure 2). We observe two unmixable copper-rich and steel-rich zones containing small spheres of opposite material (about 10  $\mu$ m in diameter). We suppose that these structures form by coagulation. The scenario of structure formation is follow. The steel-rich structures poor in copper solidify, then the structures C and F solidify when temperature reaches the value of phase separation for  $Cu_{20}Fe_{80}$  (that corresponds to maximal possible Cu solubility in stainless steel). After that D and E solidify under the phase separation temperature of  $Cu_{95}Fe_5$ .

Due to small time of interaction, distribution

of steel components at the welds respect the same proportion between them as in solid steel.

**Table 1:** Medium chemical composition of microstructures.

Structure	Element, at. %			
	Cu	Fe	Cr	Ni
“droplet”-like structure				
A	8,0	65,6	20	6,4
B	11,5	63,1	19,2	6,2
C	21,4	56,6	16,6	5,2
D	94	4,5	1,2	0,3
C2	21,3	55,2	17,2	6,3
“emulsion”-like structure				
A	0,5	70,6	20,8	8,1
B	7,9	65,7	20	6,4
C	21,3	56,5	16,5	5,7
D	94	4,5	1,2	0,3
E	91,1	5,6	2,0	1,3
F	14,9	62,5	18,0	4,6

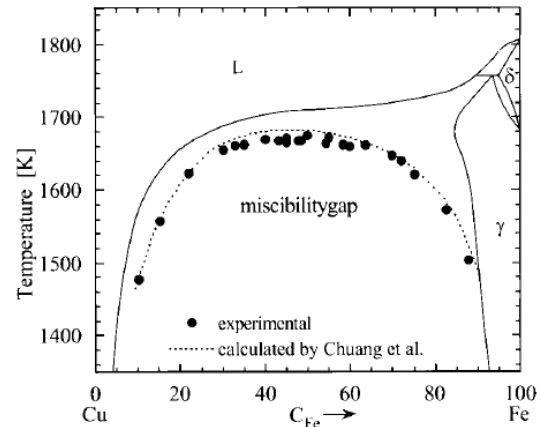


**Figure 2.** Phase diagram of Fe-Cu. The full circles correspond to the onset temperatures of phase separation reaction determined by Wilde and al. (3). The dashed curve corresponds to values calculated by Chuang and al. (4)

## 3. Model description

The model consists of rectangle containing different microstructure domains where the law of cooling, the solubility limits and diffusion coefficients depending on temperature are imposed.

Creating present model, we have introduced following simplifications:

- the model deals only with solidification period of melted zone life (after beam pass), when large structures are already formed, but they are far from equilibrium, and E-F structures do not exist yet;
- convection is neglected;
- as migration of Fe, Cr and Ni respects their proportion in steel, we consider steel as homogeneous material with diffusion characteristics of pure iron. To obtain C(M), where M = Fe, Cr or Ni, we have used  $C(M) = C_{steel} \cdot \gamma(M)$ , where  $\gamma(M)$  is the molar part of element in original steel.

### 3.1. Geometry and mesh

We have considered the rectangles with realistic dimensions: 250x200  $\mu\text{m}$  for “droplet”-like and 250x150  $\mu\text{m}$  for “emulsion”-like structures. The geometry of microstructures has been reproduced with Bezier curve instrument in total shape correspondence with SEM images.

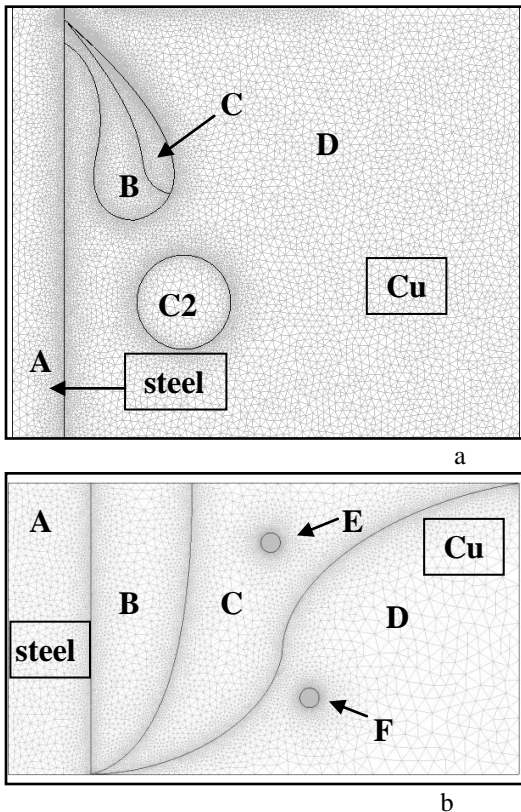


**Figure 3.** Geometry of microstructures, recreated in COMSOL media: a) “droplet”-like, b) “emulsion”-like.

The rectangles were meshed using following parameters: maximal element size of 0,3 and growing speed 1,2. The subdomains E and F have been meshed with 1  $\mu\text{m}$  and C2 - with 5  $\mu\text{m}$  maximal element sizes. The boundaries where diffusion takes place have been meshed with 1  $\mu\text{m}$  maximal element size.

### 3.2. Governing equations and initial conditions

Heat transfer in present models is governed by temporary heat equation:

$$\rho c_p \frac{\partial T}{\partial t} = \nabla(-k \nabla T),$$

where  $\rho$  is material density,  $k$ - thermal conductivity,  $C_p$  – heat capacity,  $T$  – temperature,  $t$  – time.

To avoid discontinuity in materials properties during phase transition, they have been represented by equations with Heaviside functions, which general form is:

$$A = A_{solid} + (A_{liquid} - A_{solid}) \cdot \text{flc}2\text{hs}(T - T_f, \delta T),$$

where  $T_f$  is fusion temperature and  $\delta T$  is the temperature interval of phase change (5K).

To describe appearance of spheres E and F under the temperature of phase separation, we have used other Heaviside function in these domains, which permits to pass from properties of media to properties of appearing microstructure:

$$A = A_{sphere} + (A_{media} - A_{sphere}) \cdot \text{flc}2\text{hs}(T - T_s, \delta T),$$

where  $T_s$  is the phase separation temperature.

The temperature evolution imposed to these models is brought from the results of numerical 2D model of Cu/steel electron beam welding reported in (1), where heating and convection in the melted zone have been calculated.

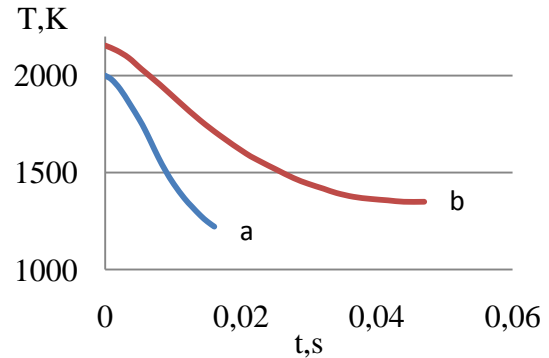


**Figure 4.** Cooling laws used in calculations: “emulsion”-type weld (a), “droplet”-type weld (b).

The present cooling curves (Figure 4) correspond to particular position in melting pool where present microstructures do form (Figure 5). They have been described by the Gauss function, but they also can be described with linear law, which is less precise but economizes the time of calculations (Table 2).

**Table 2:** Cooling laws used in calculations.

Joints	“emulsion”	“droplet”
Linear approximation : $T(K)=a \cdot t+b$		
a	-52376	-20180
b	2010,3	2069
R <sup>2</sup>	0,94	0,93
Gauss approximation :		
$T(K) = y_0 + (A/(w \cdot \sqrt{\pi/2})) \cdot \exp(-2 \cdot (t/w)^2)$		
y <sub>0</sub>	1159,264	1333,8
w	0,01523	0,0367
A	16,2814	42,6
R <sup>2</sup>	0,99	0,99

Thermal boundary conditions are follows: the corresponding cooling laws are applied for right hot wall (Figure 5) and thermal isolation condition for left wall, top and bottom of rectangle.

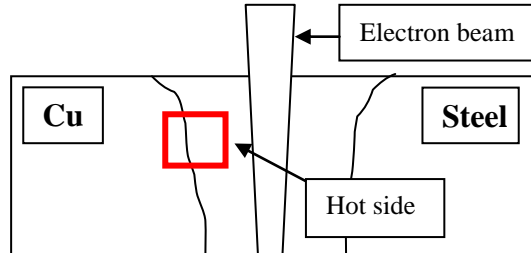


**Figure 5.** The position of modeled zone at global geometry of the weld.

To describe diffusion process we have used two different diffusion modes describing diffusion of iron in copper

$$\nabla(-D_{Cu(Fe)} \cdot \nabla C_{Cu}) = 0$$

and copper in iron

$$\nabla(-D_{Fe(Cu)} \cdot \nabla C_{Fe}) = 0,$$

where diffusion coefficients D depend on temperature

$$D_T = D \cdot \exp\left(-\frac{E}{R \cdot T}\right).$$

To rely the start of diffusion with characteristic temperatures of the system (solidus, phase separation etc.), final form of diffusion coefficients has been defined as:

$$D_{\text{domain}} = D_T \cdot f_{lc} 2hs (T_{\text{start}} - T, \delta T).$$

The subdomain and boundary conditions are presented in Table 3.

**Table 3:** Initial conditions for diffusion mode.

Subdomain conditions			
Domain	Concentration, at. %		T <sub>start</sub>
	Cu	Fe	
“droplet”-like joint			
A	0	100	T <sub>initial</sub>
B	8	92	T <sub>steel</sub>
C	18	82	T <sub>initial</sub>
D*	95	5	T <sub>s(Cu95Fe5)</sub>
C2	18	82	T <sub>initial</sub>
“emulsion”-like joint			
A	0	100	T <sub>initial</sub>
B	8	92	T <sub>initial</sub>
C**	18	82	T <sub>s(Cu20Fe80)</sub>
D*	95	5	T <sub>s(Cu95Fe5)</sub>
E**	95	5	T <sub>s(Cu20Fe80)</sub>
F**	18	82	T <sub>s(Cu20Fe80)</sub>
Boundary conditions			
droplet”-like joint		“emulsion”-like joint	
Interface	Cu, at. %	Interface	Cu, at. %
Left	0	Left	0
A/D	3	A/B	50
B/C	15	B/C	continuity
B/D	50	C/D	50
C/D	50	C/E	50
E/D	50	D/F	50
Right	95	Right	95

\* diffusion can be observed only after the moment when convection in copper media stops, which corresponds to 1370K.

\*\* - diffusion begins after separation of Cu<sub>20</sub>Fe<sub>80</sub> phase from excess of copper.

The properties of materials used in calculations are gathered in Table 4.

### 3.4. Solving method

We have used temporal General Heat Transfer Mode and two Diffusion modes (separately for copper-rich and steel-rich domains) of Comsol Multyphysics 3.4. Direct time-depended solver UMFPACK with asymmetric matrix and relative tolerance of 0.01 has been used to calculate coupled variables T, C (Fe) and C(Cu). The input time has been considered to achieve cooling to 300K.

**Table 4:** Physical constants for the materials used in calculations.

Constant	Material		
	Cu	Steel	
<b>Thermal properties</b>			
Fusion temperature, K	$T_f$	1356	1720
Phase separation temperature in Fe/Cu system*, K	$T_s$	$\text{Cu}_{95}\text{Fe}_5$ 1370	$\text{Cu}_{20}\text{Fe}_{80}$ 1550
Density (solid), $\text{kg}/\text{m}^3$	$\rho_s$	8700	7980
Density (liquid), $\text{kg}/\text{m}^3$	$\rho_l$	7940	7551
Heat capacity (solid), $\text{J}/(\text{kg}\cdot\text{K})$	C	385	433
	$P_s$		
Heat capacity (liquid), $\text{J}/(\text{kg}\cdot\text{K})$	C	350	734
	$P_l$		
Thermal conductivity (solid), $\text{W}/(\text{m}\cdot\text{K})$	$k_s$	400	8.116
Thermal conductivity (liquid), $\text{W}/(\text{m}\cdot\text{K})$	$k_l$	140	12.29
<b>Diffusion properties</b>			
Diffusion coefficient, $\text{m}^2/\text{s}$	D	$3\cdot 10^{-4}$	$1.4\cdot 10^{-4}$ **
Activation energy, $\text{kJ}/\text{mol}$	E	255	217 **

\*- adjusted to Cu/steel system.

\*\*- data for Fe.

## 4. Results and discussions

### 4.1. Comparison of results when linear and gauss cooling laws

We have compared the element distribution when gauss and linear approximation of temperature field is applied and have found that there is good coincidence as between them (for example, Figure 6). Below, we show results for linear approximation. The coincidence between calculated concentration profiles and experimental data confirms that present temperature distribution is more or less realistic.

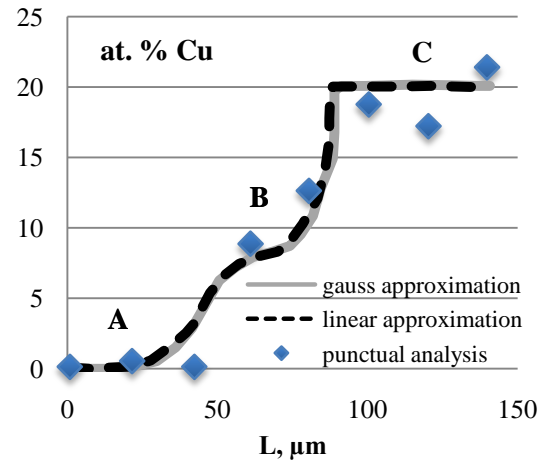


**Figure 6.** Comparison between Cu concentration profiles in steel-rich zones (A,B,C) of “emulsion”-like microstructures obtained using gauss and linear cooling law with the results of local SEM-ESD analysis.

### 4.2. Principal results

We have obtained the concentration fields developing on time, which characteristic concentration profiles are presented at Figures 7 and 8. Profiles of Ni are not shown due to its small concentration.

For “emulsion”-like weld, diffusion of Cu from B to A and from C to B begins immediately after beam pass, resulting on large diffusion distances and slow change of copper concentration. The lifetime of melted zone is very small (0,012 s), and undercooling phenomena take place. When the system reaches the temperature corresponding to solidus in equilibrium condition, at the zone C excess of copper begins to form copper-rich globules E and in zone D steel-rich globules F form. At the temperature of 1550 the phase  $\text{Cu}_{20}\text{Fe}_{80}$  (steel saturated with copper in our case) solidifies, and from this moment diffusion starts on interfaces C/E and D/F resulting on fine diffusion distances observable in SEM. At the same time when C is already solid and D – liquid, Cu diffuse from D to C, but diffusion of steel components in copper is not observable due convection in D. At 1370K copper-rich D ( $\text{Cu}_{95}\text{Fe}_5$ ) solidify, and we observe insignificant diffusion of steel components from C to D.

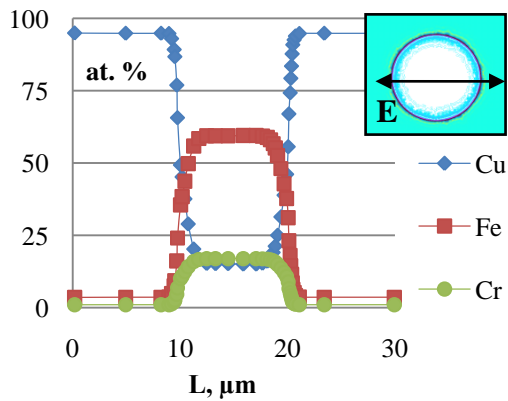
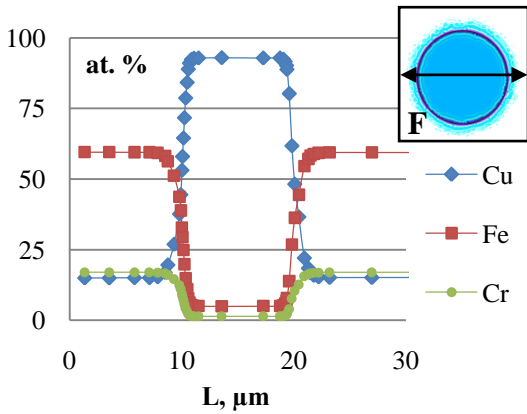
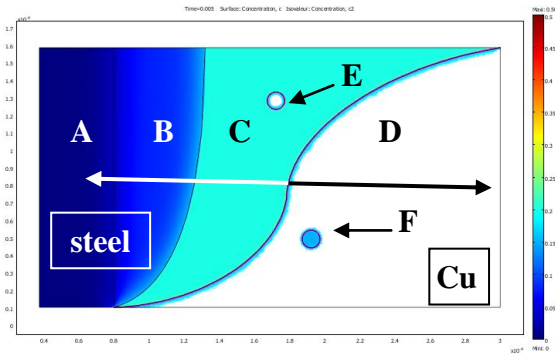
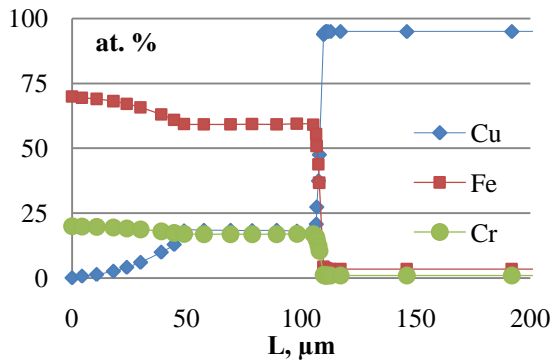


**Figure 7.** Concentration fields and profiles for “droplet”-like structures.

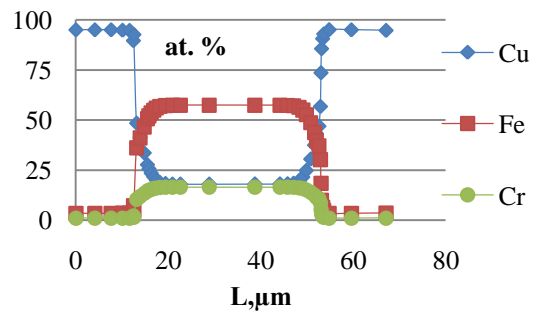
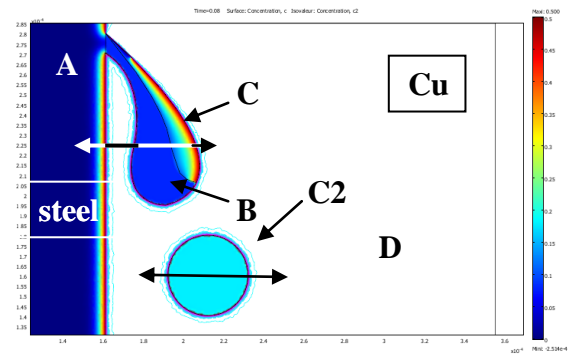
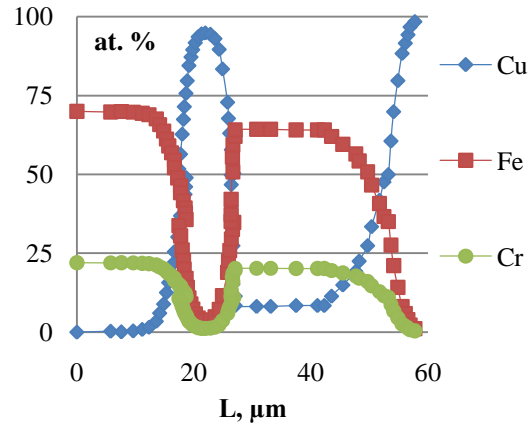


**Figure 8.** Concentration fields and profiles for “emulsion”-like structure.

For “droplet”-like weld, diffusion of copper from D to A starts immediately. As steel droplet supposed to be teared away by copper flux, it moves, and so it stops after  $T_f$  of steel., so diffusion of copper into B starts from this moment. Otherwise, the copper flux attacking the droplet from the top interacts with C from initial temperature. Teared away droplet C2 is the final product of this interaction: entire domain is saturated with copper, and thin diffusion interface formed after droplet solidification ( $Cu_{20}Fe_{80}$ ) is observable. After solidification of D ( $Cu_{95}Fe_5$ ) weak diffusion of

steel components into copper media take place. Lifetime of melted zone is almost three times longer (0,035s) than for “emulsion”-like joint due to domination of copper in welding pool.

#### 4.2. Validation of model

To validate the models, we have compared calculated concentration profiles with real concentrations founded from linear SEM-ESD analysis and found good correspondence of these data. As an example, the profiles of calculated and determined copper concentration are shown at Figure 9.

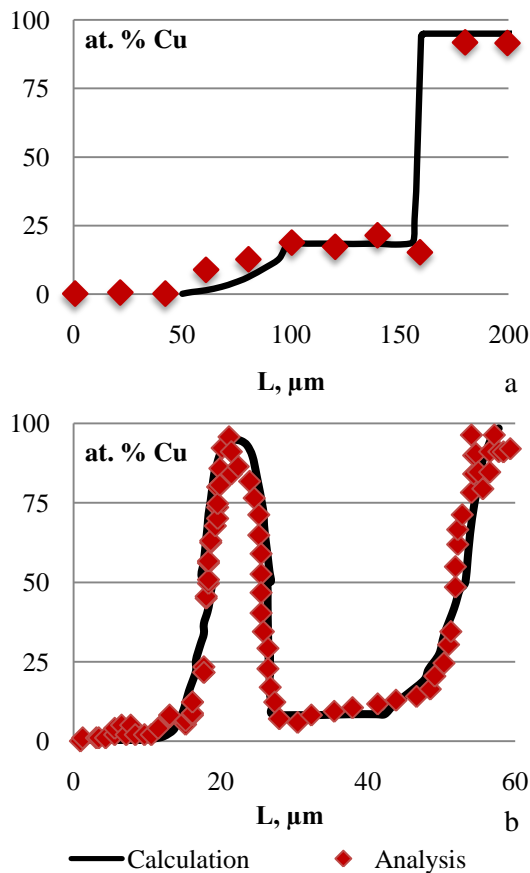


**Figure 9.** Comparison between calculated profiles and real copper concentration founded by SEM-ESD analysis in “emulsion”-like (a) and “droplet”-like (b) microstructures.

Other manner to validate diffusion models is to compare observable and calculated diffusion distances. In our model, where diffusion is represented separately for copper-rich and steel-

rich domains, total diffusion length was considered as summa of diffusion length of copper in steel and of iron in copper.

**Table 5:** Diffusion distances calculated and observed on different interfaces.

Interface	Distance, $\mu\text{m}$	
	“droplet”-like	
	calculated	observed
A/D	14	17
B/D	4	3
C/D	4	3
C2/D	2,4	1,8
Interface	“emulsion”-like	
	calculated	observed
	A/B	31
C/D	1,7	1,4
C/E	1,3	1,1
D/F	1,7	2,3

Several diffusion interfaces (as B/C ) are not observable in SEM images due to insignificant change of composition. The observable diffusion lengths are in good correspondence with calculated ones.

#### 5. Conclusions

Present numerical models of microstructures development are in good correspondence with SEM images and the results of local ESD analysis. They confirm that temperature evolution, which was taken from our previous numerical model (1), is realistic, and also our hypothesis on the way of microstructure formation under different welding conditions.

#### 6. References

- <sup>1</sup> I. Tomashchuk, P. Sallamand, J-M. Jouvard. CD de Journée thématique « *Modèles de transfert – thermocinétique* » de Société Française de Thermique, 24 janvier 2008, Le Creusot, France.
- <sup>2</sup> N.P. Lyakichev. *Les diagrammes des phases des systèmes métalliques binaires*. Moscow, Machinostroenie (1996).
- <sup>3</sup> G.Wilde, J.H. Perepezko, *Acta materialia*, **47**, 3009-3021 (1999)
- <sup>4</sup> Y.-Y.Chuang, R. Schmid, Y.A. Chang, *Metallurgical Transactions*, **15A**, 1921 (1984)